energy&fuels

pubs.acs.org/EF

Article

Kinetic Experiments and Modeling of High-Temperature Sulfidation Corrosion in Oil

Ishan P. Patel, Gheorghe Bota, and David Young*

Cite This: *Energy Fuels* 2025, 39, 1844−1855

Read Online

ACCESS | Metrics & More | Article Recommendations

ABSTRACT: High-temperature sulfidation corrosion of steel in oil refineries has long been postulated to proceed via a solid-state reaction mechanism for which parabolic mass loss versus time trends are typically observed if the overall process is diffusion controlled. However, a linear trend has been observed for oil phase corrosion of carbon steel by dodecylsulfide in a flow-through reactor, implying interfacial reaction control. A kinetic equation for the interfacial reaction is incorporated into a general solid-state model by relaxing the assumption of interfacial equilibria to capture the observed linear trend. The kinetic framework depicted herein can explain whether linear or parabolic kinetics would be observed based on the reactivity of organosulfur compounds.

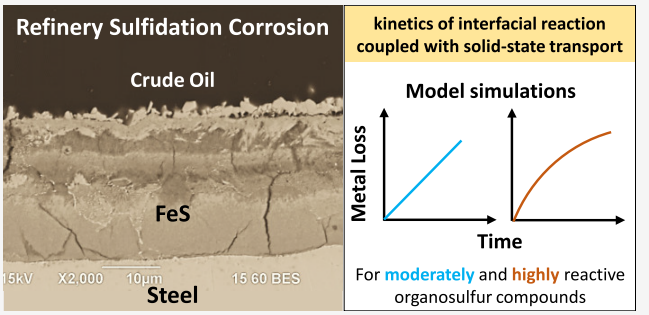

INTRODUCTION

Refinery distillation units suffer from high-temperature sulfidation corrosion by organosulfur species in crude oils, which begins at temperatures as low as 260 °C (480 °F).[1−3] Catastrophic failures have occurred due to severe sulfidation corrosion resulting in worker injury, jeopardizing the safety of surrounding communities, endangering the environment, and incurring huge economic losses.[4−6] All of the commonly used alloys for constructing refinery equipment, viz., austenitic stainless steels, Cr−Mo steels, and carbon steels, are affected by oil phase sulfidation corrosion with increasing vulnerability.[1,3,7−11] Although Cr-containing steels provide better protection against sulfidation, carbon steel is still widely used in high-temperature units of oil refineries. Commonly used corrosion prediction tools in industrial guidelines, such as McConomy curves, have an order of magnitude of uncertainty since the field corrosion data used to draw these curves are highly scattered.[3,8,12] Therefore, instead of such empirical tools, a mechanistic corrosion model is highly sought for accurate prediction of sulfidation rates of carbon steel in the high-temperature sections of oil refineries.[10,11,13−16]

Every crude oil consists of a unique composition of numerous organosulfur species, mainly categorized into thiols, dialkylsulfides, and thiophenes, in order of decreasing reactivity.[1,17−20] Refinery operators have long presumed that organosulfur species must convert to H_2S to embark the sulfidation reaction with steel.[21] However, Foroulis showed that dialkylsulfides and mercaptans could directly react with steel without being converted to H_2S.[1,22] Considering the nonstoichiometry of the sulfidation reaction product of crystalline iron sulfide, pyrrhotite ($Fe_{1-x}S$), Foroulis proposed a solid-state chemistry based corrosion mechanism.[1,22] This mechanism involves the adsorption of organosulfur molecules on the surface of iron sulfide and subsequently their catalytic decomposition to induce cation vacancies and electron holes in the generated iron sulfide, which transport toward the steel-iron sulfide interface and get annihilated.[1,8] Nevertheless, no experimental evidence has been found supporting the steps of adsorption and catalytic decomposition of organosulfur compounds during sulfidation corrosion.[1] Jin et al. proposed a slightly different mechanism for sulfur incorporation and vacancy formation in iron sulfide.[1,13] The transport of iron, mimicked by cation vacancies, was assumed to be rate limiting by Jin et al., which could be supported by the sulfidation kinetic data published earlier.[13,23] However, the kinetic data presented in this work suggest that the interfacial reactions generating cation vacancies and holes could be rate limiting.

In general, it can be inferred that the mechanism of oil phase sulfidation corrosion consists of the generation of charged defects in crystalline iron sulfide at the iron sulfide-oil interface, their transport toward the steel−iron sulfide interface in the solid state, and annihilation by iron incorporation therein.[1,8,13] Generation and annihilation of charged defects occur via reactions at the respective interfaces. This mechanism for oil

Received: October 17, 2024
Revised: January 9, 2025
Accepted: January 10, 2025
Published: January 20, 2025

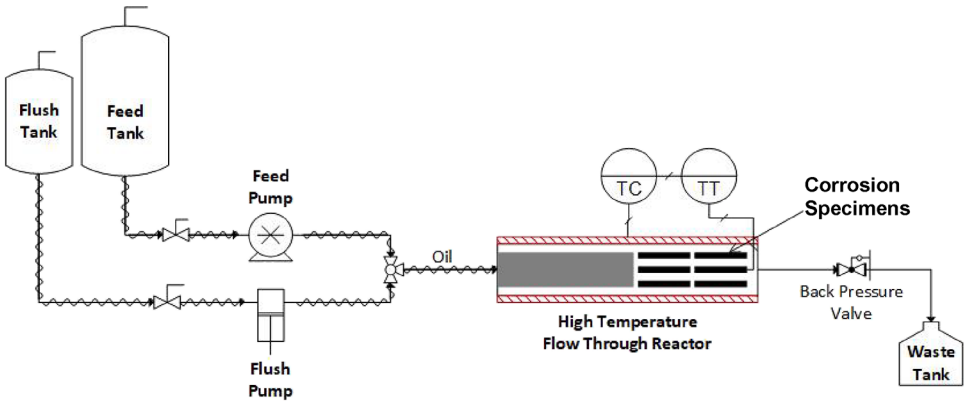

Figure 1. Schematic diagram of experimental apparatus - flow through mini autoclave (FTMA).[13,28,41] Reproduced from ref 41. Copyright 2024 Publisher ACS Publications.

phase sulfidation corrosion is formalized in this work using Kröger-Vink notations,[24−26] which is in conformance with the widely accepted theory of solid-state metal oxidation.[25,27] It is also shown further that the use of Kröger-Vink notations facilitates the incorporation of interfacial kinetics into the framework for solid-state transport of vacancies and holes.[24−26] Since our experimental kinetic data on the sulfidation of carbon steel indicate that interfacial processes could also be rate limiting, their kinetics need to be incorporated into the general solid-state kinetics framework.[15,23,28]

Kinetics of high-temperature solid-state corrosion can be experimentally analyzed by measuring mass gain by solid corrosion product or mass loss by metal specimen, with respect to time. If the overall process is controlled by solid-state transport of the cation vacancies and holes, the growth rate of corrosion product layer thickness (X) diminishes as resistance imposed by the layer increases, viz., $dX/dt \propto 1/X$; integration of this relation leads to a parabolic law, i.e., $X = k_p\sqrt{t}$.[29] If the overall process is controlled by interfacial reactions, the growth rate of the layer thickness remains constant with increasing thickness of the corrosion product layer, viz., $dX/dt \approx k_l$; time-integration leads to the linear law, i.e., $X = k_l t$.[30]

As most research in this area has been done by the refining industry, much of the collected data is unavailable to the public. A few comprehensive studies on oil phase sulfidation corrosion can be found in the literature. Qu et al. measured the mass of iron sulfide formed on carbon steel by a dimethyl disulfide (DMDS) oil solution during several static autoclave experiments of specific durations at 270 °C.[23] The nonlinear "mass-gain" versus time curve traced from these experimental data points was identified as parabolic by Qu et al.[23] It should be noted that the choice of model sulfur compound, DMDS, and the test temperature of 270 °C are not representative of the conditions in the high-temperature units of oil refineries. El Kamel et al., found a logarithmic mass loss versus time trend for autoclave sulfidation experiments on carbon steel when iron sulfide thickness was in the range of a few nanometers.[15] At higher thicknesses, the trend was reported to be parabolic.[15] The experiments by El Kamel et al. were performed at 300 °C using a real crude oil containing natural organosulfur species, closely representing refinery conditions.[15] However, real crude oil also contains naphthenic acids which are known to dissolve carbon steel and concurrently produce iron oxide, especially in the presence of iron sulfide.[31,32] This means that some fraction of the total mass loss of carbon steel measured by El Kamel et al. could be attributed to the naphthenic acid corrosion, but this was unaccounted.[12,15,31−35] The presence of iron oxide was acknowledged by El Kamel et al., which may have also influenced the kinetics of sulfidation corrosion.[12,15,35,36] Comprehensive sets of kinetic experiments for sulfidation corrosion have demonstrated the need to further address limitations surrounding previous experimental work by choosing dodecylsulfide to represent organosulfur species in crude oil and the temperature of 343 °C, typical for sections of oil refineries suffering severe sulfidation corrosion. The most important outcome of the presented experimental work is the linear dependence of mass loss of carbon steel versus time, for which the mechanistic explanation and kinetic modeling have been provided in the latter part of this paper.

EXPERIMENTAL METHODOLOGY

In oil refineries, sulfidation corrosion is also influenced by the concurrent phenomenon of naphthenic acid corrosion.[34,37,38] It has been postulated for the present isolated experimental study of sulfidation corrosion that the fundamental solid-state mechanism of corrosion also holds in the presence of naphthenic acids. This postulate provides a rational basis for choosing an isolated study of sulfidation corrosion in the absence of naphthenic acid corrosion.

Static autoclaves are commonly used to perform oil-phase high-temperature sulfidation corrosion experiments.[15,23,39,40] However, the concentration of organosulfur species in the liquid phase decreases during an autoclave experiment, mainly due to consumption in corrosion and thermal decomposition into H_2S, which partitions into the vapor phase. A false parabolic mass loss versus time trend may be observed simply due to the decreasing concentration of organosulfur compounds in the liquid phase of a static autoclave. Therefore, the static autoclave is not suitable for accurate kinetic experiments. In this work, sulfidation experiments are performed in a flow-through reactor, which enhances the convective mass transport of corrosive molecules. The flow reactor also avoids the accumulation or depletion of reactants and products in the oil phase. Also, the relatively short residence time of the oil solution containing organosulfur species in the flow reactor at high temperatures mitigates adverse experimental impacts associated with the thermal decomposition of corrosive molecules. Experimentally observed depletion of the liquid phase organosulfur concentration during the pass was less than 2% in all experiments.

A carbon steel material was selected for sulfidation experiments given its formation of the less chemically complex corrosion product pyrrhotite $Fe_{1-\delta}S$.[15,40] The outer layers of corrosion products formed on carbon steel specimens during any isothermal period usually detach by the combined action of cooling and flushing. Therefore, mass loss was used to calculate sulfidation rates instead of mass gain.

https://doi.org/10.1021/acs.energyfuels.4c05072
Energy Fuels 2025, 39, 1844−1855

Table 1. Chemical Composition (wt.%) of Carbon Steel Specimens[13]

C	Si	Mn	P	S	Cr	Ni	Mo	V	Cu	Fe
0.18	0.41	0.8	0.11	0.06	0.02	0.04	0.02	0.03	0.08	balance

Kinetic investigations were performed by manipulating the time and organosulfur concentration. The main parameter of interest was the duration of the experiment to determine whether sulfidation corrosion was in control of interfacial reactions or solid-state diffusion.

Experimental Apparatus. The sulfidation experiments were conducted in a high-temperature reactor called a flow-through-mini-autoclave (FTMA), with a flow rate of 1.5 cc/min, as illustrated in Figure 1. The FTMA setup comprises a high-temperature, high-pressure reactor, two feeding tanks, dedicated pumps for supplying mineral oil and the test solution, and a waste tank. The test solution, containing a model sulfur compound, was supplied from the feed tank, while mineral oil used for the preheating and flushing stages was supplied from a flush tank, as shown in Figure 1. A three-way valve was employed to switch between the oil feeds. Temperature measurement was carried out by using a thermocouple inserted into the reactor near the specimens. The thermocouple and heating coil around the reactor were connected to the temperature controller. Pressure within the reactor was regulated by a back-pressure valve at the reactor outlet to maintain a full liquid phase.

Analytical Instruments. The concentration of sulfur in the model oil solution was measured using X-ray fluorescence spectroscopy with an XOS Petramax instrument. A JEOL JSM-6390 scanning electron microscope (SEM) was used to analyze morphologies and cross sections of the solid corrosion product. Elemental analysis of scale cross sections was performed using a Bruker energy dispersive spectroscopy (EDS) analyzer. X-ray diffraction patterns for the solid corrosion products were collected with a Rigaku Miniflex 600 X-ray diffractometer at a scanning rate of 3 degrees of 2θ per minute, with a step width of 0.02 degrees of 2θ and CuK_{α} radiation generated at 30 kV and 15 mA.

Materials. Oil solutions containing the model organosulfur compound were prepared in the clear paraffinic mineral oil Tufflo 6056 supplied by Citgo. Dodecylsulfide (DDS)[13] was used as the model organosulfur compound used to cause sulfidation corrosion of carbon steel specimens, considering its high reactivity. Rectangular carbon steel corrosion specimens of dimensions 15.9 × 15.2 × 0.6 mm with a central hole of diameter 3.8 mm were used. The chemical composition of the carbon steel specimens is given in Table 1.[13] The specimens were successively polished with Indasa Rhynogrip White Line 400 and 600 grit abrasive papers under a continuous flow of 2-propanol and dried by blowing with inert gas. The dimensions of the specimens were measured by using a Vernier caliper. The weights of the specimens before and after the sulfidation experiment were measured using an XPR205 Mettler Toledo analytical balance. One of the specimens was embedded in a clear epoxy for cross-sectional SEM-EDS analyses.

Experimental Matrices. The following tables describe conditions for sulfidation corrosion experiments reported herein with varying time (Table 2) and concentration of DDS (Table 3).

Experimental Procedure. The preparation of the test solution for each experiment involved adding a specific concentration of DDS into mineral oil in a 2 L glass beaker. The mixture was heated on a hot plate at temperatures below 60 °C and continuously stirred to aid in the solvation of corrosive compounds. The solution was then poured into the feed tank of the FTMA well before each experiment. In each experiment, four carbon steel specimens of known mass and dimensions were used: two for assessing mass loss, one for surface analysis via SEM and XRD, and one for cross-sectional analysis via SEM and EDS. The specimens were polished with 400 and 600 grit polishing papers under a continuous stream of isopropanol. The specimens were placed on the holder and loaded into the FTMA reactor, which was then connected to the FTMA loop.

Table 2. Evaluation of Sulfidation Rate versus Time to Ascertain that It Remains in the Interfacial Reaction Control

durations (h)	concentration of DDS as total sulfur (wt %) in mineral oil	corrosion specimens	temperature (°C)	pressure (kPa)
3, 6, 9, 12, 15, 18, 24, 36, and 48	0.25	carbon steel	343	600

Table 3. Evaluation of Sulfidation Rate versus DDS Concentration

concentrations of DDS as total sulfur (wt %) in mineral oil	corrosion specimens	temperature(°C)	pressure(kPa)	durations (h)
0.1, 0.25, 0.45, and 0.625	carbon steel	343	600	24

Initially, the reactor was run cold, pushing mineral oil to fill the reactor and all of the lines. Then the electric heating coil wrapped around the reactor was turned on, and the temperature was gradually raised to 343 °C (650 °F) while mineral oil was still flowing through the reactor. Once the experimental temperature was achieved, the feed was switched from mineral oil to the organosulfur solution at a flow rate of 1.5 cc/min. The sample is thus instantly exposed to the corrosive solution at the required temperature, avoiding unwanted heating and cooling cycles in the presence of corrosive species. At the conclusion of the experiment, the feed returned to Tufflo for flushing for 1 h. The reactor was turned off with mineral oil continuing to flow through it for cooling. Finally, the system was turned off after 10 min.

After the reactor cooled to room temperature, corrosion specimens were extracted and meticulously cleaned by stepwise dipping them into toluene-containing beakers while retaining the corrosion product on the surface. The mass of each of the two specimens was measured after the oil was removed, dry rubbing of the corrosion product, and chemically removing the corrosion products with Clarke solution according to ASTM G1−03. The corrosion rate was determined by dividing the average difference in the initial and final masses of two specimens by the experiment duration. The third specimen was used for surface analysis, and the fourth specimen was embedded in epoxy for cross-sectional analysis.

RESULTS AND DISCUSSION

The kinetics of sulfidation corrosion was elucidated by conducting a series of corrosion experiments by manipulating time and organosulfur concentration.[28] The evolution of sulfidation rates is shown by the mass loss of corrosion specimens, instead of corrosion rate, because the popular terms related to kinetics, such as parabolic, para-linear, and linear, pertain to the relationship between mass loss and time.[28] It can be observed from the mass loss versus time plot in Figure 2 that the sulfidation rate, represented by the slope of the plot, remained constant for the first 48 h. This means that sulfidation corrosion remained in interfacial reaction control during this initial period.[28] The trend aligns with our premise that the sulfidation reaction was not governed by diffusion control, which would have otherwise yielded a parabolic trend instead of linear. The short-time mass loss data (<3 h) are not plotted in Figure 2 because of large error margins in measured values. However, a nonlinear relationship between mass loss versus time can be imagined therein because the regression line

https://doi.org/10.1021/acs.energyfuels.4c05072
Energy Fuels 2025, 39, 1844−1855

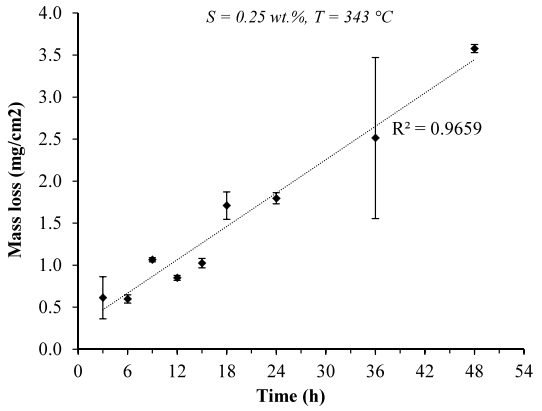

Figure 2. Mass loss versus time data of sulfidation corrosion of carbon steel by 0.25 wt % of sulfur by DDS in model oil solution at 343 °C.[28]

does not pass through the origin in Figure 2. This region may be explained by interfacial reaction control and charging due to undeveloped space charge at the interfaces at a lower thickness of iron sulfide.[42]

The 24 h sulfidation rate of carbon steel specimens by dodecylsulfide (DDS) demonstrated a linear correlation with respect to the concentration, as shown in Figure 3. It is not

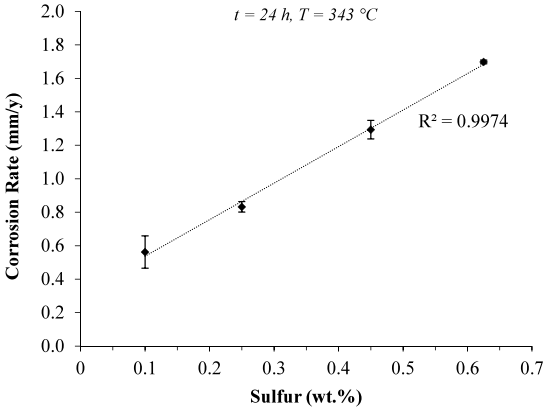

Figure 3. Corrosion rate versus concentration data of sulfidation corrosion of carbon steel for 24 h by DDS in model oil solution (expressed as wt % S from DDS) at 343 °C.[28]

appropriate to assign reaction orders to heterogeneous reactions because they are unlikely to be elementary.[43] A nonlinear curve can be envisaged at lower concentrations since the regression line does not pass through the origin in Figure 3. The pyrrhotite formed by the lower concentration of model organosulfur compounds may have lower amounts of charged defects.[44] Consequently, the size of the space charge region would be larger simply due to the lack of charges required for screening of electric field across the interfaces. It is speculated that the kinetics of interfacial reactions with an electrochemical nature are responsible for such a nonlinear trend at lower concentrations. The lower limit of the concentration range selected here represents typical sulfur content in crude oils, and the upper limit is decided by the ease of dissolving DDS in mineral oil.

The characterization of the corrosion product was performed for the analysis of the morphology, chemical composition, and crystal structure type. Representative scanning electron microscopy (SEM) images are shown in Figure 4 as the morphology of the corrosion product was characteristically similar between experiments. SEM images

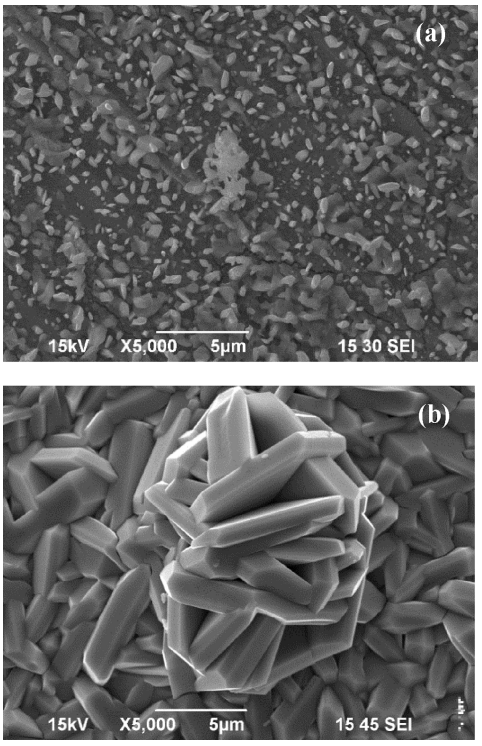

Figure 4. Morphological analysis of corrosion product formed after 24 h on the carbon steel surface by 0.625 wt % S from DDS using scanning electron microscopy (SEM); (a) inner layer attached with metal surface and (b) outer layer exposed to oil.

shown in Figure 4 capture freshly formed pyrrhotite crystals on a specimen surface, supporting the hypothesis that the growth of iron sulfide primarily occurs through the outward diffusion of iron.[28] In Figure 4, image (a) shows the inner layer and (b) shows the outer layer of pyrrhotite formed by the captioned experimental conditions. These images show the difference between the size of the pyrrhotite crystals, which may be explained using decreasing Gibbs free energy difference during sulfidation corrosion. In the beginning, a steep thermodynamic potential gradient exists to promote more nucleation and less growth, which is depicted by small crystals in the inner layer of the product in Figure 4a. With the increasing thickness of the iron sulfide layer, the thermodynamic potential gradient gradually becomes shallow, promoting crystal growth as demonstrated by large crystals in the outer layer of the product in Figure 4b.

Analyzing the corrosion product through energy dispersive X-ray spectroscopy (EDS) confirmed the presence of iron and sulfur in the corrosion product layer, as shown in Figure 5. The epoxy embedding of the coupon resulted in the disbonding of the corrosion product layer from the metal surface, with the resin filling the gap. The detection of carbon and oxygen in dark regions during the EDS scanning, as shown in Figure 5, provides evidence for that.

The crystalline phases in the layer were characterized by using X-ray diffraction (XRD). The peaks observed in the pattern were identified as iron and nonstoichiometric pyrrhotite-type hexagonal iron sulfide (PDF 01−080−1026),[45] as illustrated in Figure 6. Disproportionate relative

https://doi.org/10.1021/acs.energyfuels.4c05072
Energy Fuels 2025, 39, 1844−1855

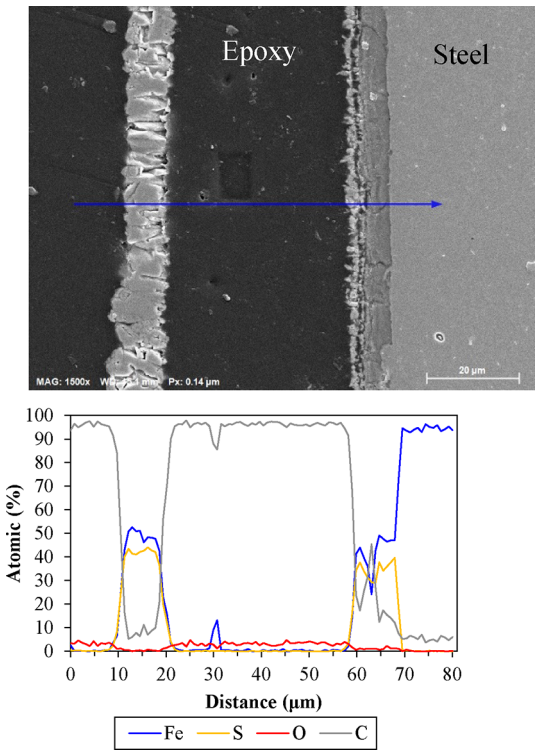

Figure 5. Analysis of corrosion product formed on carbon steel surface by DDS (0.625 wt % of sulfur) after 24 h by energy dispersive X-ray spectroscopy (EDS), in scanning line mode.

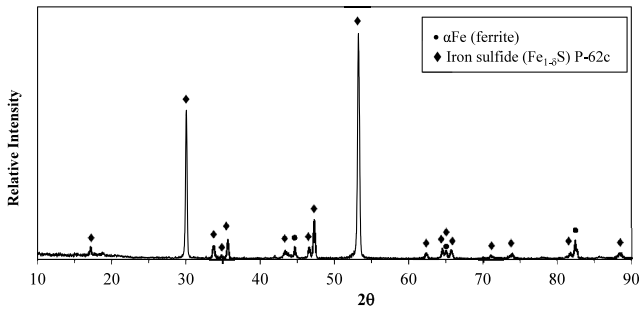

Figure 6. X-ray diffraction pattern of corrosion specimen with corrosion product formed after 24 h on carbon steel surface by 0.625 wt % S from DDS

intensities of the major peaks indicate preferential iron sulfide surface growth in certain crystallographic directions, as exhibited by the faceted morphological features observed in the SEM images.

MECHANISM

A solid layer of iron sulfide is produced on the steel surface during oil phase high temperature sulfidation corrosion as described by the below chemical reaction.[28]

$$(1-\delta)Fe_{(s)} + RSR_{(oil)} \rightarrow Fe_{1-\delta}S_{(s)} + RR_{(oil)} \quad (1)$$

Here, R is an aliphatic moiety or a hydrogen. The nonstoichiometric chemical formula of iron sulfide ($Fe_{1-\delta}S$) indicates deficiency of iron, typical for pyrrhotites.

The direct sulfidation reaction of organosulfur species with the fresh metal surface ceases immediately by the nucleation of corrosion products thereon, which rapidly cover the metal surface. Thus, the metal−oil interface splits into two: metal−metal sulfide and metal sulfide−oil. Consequently, the overall sulfidation reaction (1) must also split into two "half" reactions at the metal−metal sulfide and metal sulfide−oil interfaces, incorporating iron and sulfur into iron sulfide, respectively. The connectivity between the two interfacial reactions is maintained by the solid-state "atomic" transport of iron and sulfur through iron sulfide.

X-ray diffraction analysis confirmed that the iron sulfide produced in oil phase sulfidation corrosion is pyrrhotite, with vacancies in its Fe lattice positions.[15,40,46] Since pyrrhotite is a crystalline ionic solid with some degree of covalency,[46] it is also customary to describe iron and sulfur in the crystal structure of pyrrhotite as cations and anions, respectively. Significant cation (iron) vacancies in the crystal structure imply that the layer predominantly grows by outward diffusion of iron.[25] This assertion can be supported by the clusters of newly nucleated iron sulfide crystals observed during the surface analysis of the iron sulfide layer by electron microscopy, as shown in Figure 4. Atomic diffusion of iron in pyrrhotite occurs by the vacancy mechanism, in which iron jumps into an adjacent cation vacancy. These jumps create an opposite movement of cation vacancies which are accompanied by the movement of electron holes.

Since solid-state interfacial reactions involve the "transfer" of vacancies across interfaces, along with stoichiometry and charges, a special notation system is necessary to enable their balancing across the reaction equation. Therefore, interfacial reactions are described using Kröger−Vink notations, which are commonly adopted in the field of solid-state defect chemistry.[24,25,47,48] These notations facilitate the depiction of interfacial reactions in terms of charged point defects, which is more realistic than a conventional description using ions (Fe^{2+}, S^{2-}) and electrons (e^-) by traditional notations.

It may be considered that the removal of iron from a hypothetically perfect iron sulfide crystal would cause structural relaxation of adjacent lattice elements in such a way that this vacancy assumes negative charge by "accepting" electrons from the valence band causing a local polarization.[46,49−51] Hence, positive electron holes are created in the valence band.[44] Since the charges of the point defects are the result of a local polarization relative to the perfect charge neutral crystal, they are denoted using (′) and (•) for negative and positive charges, respectively, instead of (−) and (+).[24,47,49] Accordingly, the negative iron vacancy (V) and the positive holes (h) can be denoted by V''_{Fe} and $h^{\bullet}$, respectively, as per Kröger−Vink notations.[24,47,49] Here, the subscript Fe indicates any cation site in the lattice.

The overall mechanism of sulfidation corrosion is illustrated schematically in Figure 7 and the individual steps are described further.

(I) Generation of charged point defects at the iron sulfide−oil {O} interface[1,25,47]

The addition of sulfur to the iron sulfide layer, from organosulfur parent molecules (represented as RSR) in crude oil, generates cation vacancies and electron holes in iron sulfide at the iron sulfide−oil {O} interface as shown by reaction 2.[1,25,47]

$$RSR + Fe_{Fe} \rightarrow (FeS) + V''_{Fe} + 2h^{\bullet} + RR \quad (2)$$

Here, "atomic" iron leaves its lattice position to bond with the newly incorporated sulfur at the surface, indicated by (FeS), and creates a cation vacancy. As explained earlier, this cation vacancy induces structural relaxation, creating positive

https://doi.org/10.1021/acs.energyfuels.4c05072
Energy Fuels 2025, 39, 1844−1855

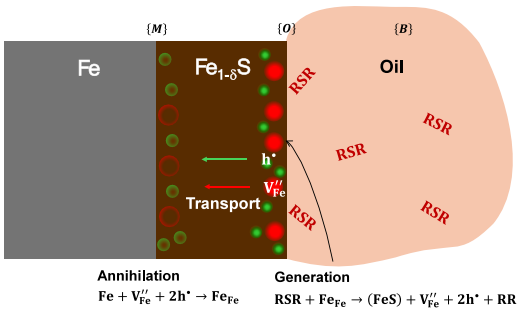

Figure 7. Mechanistic steps of the solid-state sulfidation corrosion of steel by crude oil.

holes. It can be observed that lattice vacancies do not balance on both sides of reaction 2 because V''_{Fe} was created by plugging a "virtual" surface vacancy $V^{\times}_{Fe}$ beside newly formed (FeS); surface vacancy $V^{\times}_{Fe}$ is omitted from reaction 2 by convention.[47]

(II) Transport of charged point defects from the iron sulfide−oil {O} to iron−iron sulfide interface {M}[25,47]

Cation vacancies V''_{Fe} and electron holes $h^{\bullet}$ move inward through the solid crystals of pyrrhotite due to the gradients of their electrochemical potentials across the iron sulfide layer.

(III) Annihilation of charged point defects iron−iron sulfide interface {M}[1,25,47]

Cation vacancies V''_{Fe} and electron holes $h^{\bullet}$ are annihilated at the iron−iron sulfide interface {M}, as shown by the reaction below.

$$Fe + V''_{Fe} + 2h^{\bullet} \rightarrow Fe_{Fe} \quad (3)$$

Note that the original source of Fe is steel, which is a crystalline material. This means that filling of V''_{Fe} by Fe (as shown in reaction 3 should create a vacancy of Fe in steel $V^{\times}_{[Fe]}$. The square brackets are used to denote the lattice position of Fe in steel. Subsequently, reaction 3 can be rewritten as shown below.[26]

$$Fe + V''_{Fe} + 2h^{\bullet} \rightarrow Fe_{Fe} + V^{\times}_{[Fe]} \quad (4)$$

Two possible mechanisms, generally described as injection and coalescence, can be described for the fate of the surface vacancies in steel $V^{\times}_{[Fe]}$.[52] If surface vacancies disperse into the metal, they may eventually get entrapped at grain boundaries or simply "vent off" from the opposite metal surface.[26,52] A unilateral outward growth of pyrrhotite with almost a stagnant iron−iron sulfide interface occurs due to such vacancy injection. This scenario is assumed to be unlikely due to low diffusivities of vacancies in α-Fe at lower temperatures.[53,54] If $V^{\times}_{[Fe]}$ are relatively immobile, such a depleted metal surface may undergo reconstruction by coalescing of surface vacancies $V^{\times}_{[Fe]}$ to accommodate sulfur, allowing inward growth of pyrrhotite.[52,55−58] This mechanism explains the bilateral growth of pyrrhotite with both interfaces moving with respect to the original steel surface. Vacancy coalescence and surface reconstruction are practically indistinguishable processes. It is assumed that the surface reconstruction kinetics is significantly rapid compared to diffusion or interfacial reactions. Since pyrrhotite growth occurs predominantly by outward diffusion of iron as depicted by Figure 4, only the interfacial reactions 2 and 3 as well as related diffusion of defects are modeled for kinetics.

KINETICS

As explained in the previous section, the solid-state sulfidation corrosion mechanism consists of interfacial reactions and the transport of charged defects. Kinetic modeling of the transport part can be considered fairly resolved considering the applicability of Wagner's theory of oxidation.[25,59−63] According to this theory, the oxidation of metal proceeds by solid-state coupled diffusion of ionic and electronic species under the thermodynamic potential gradients established by the interfacial reactions.[59] The most imperative feature of Wagner's theory is a theoretical derivation of experimentally observed parabolic mass loss/gain versus time curve by assuming coupled currents condition and interfacial equilibria.[29,59] The conditions of coupled currents and interfacial equilibria adopted in Wagner's derivation need further discussion pertaining to their applicability to oil phase sulfidation. Initially, during interfacial charging, the coupled current condition is not valid until the space charge is fully developed.[26,64] The coupled currents condition is effective only after the sulfide thickness becomes greater than the sum of Debye screening distances from both interfaces, known as the "thick film regime".[42,64,65] However, this charging period is quite short in sulfidation corrosion because pyrrhotite, the corrosion product of sulfidation corrosion, is a good conductor for charged defects and accommodates a high density of defects due to a higher degree of nonstoichiometry.[25,46,66,67] Therefore, long-term oil phase sulfidation can be modeled as "thick film" corrosion by adopting the coupled current condition. In this thick film regime, the assumption of interfacial equilibria is invalid if free energy dissipated by the interfacial reactions is significantly higher than for diffusion,[26,28,30] In such a case, the linear relation of mass loss versus time is observed if interfacial reaction kinetics is slower than diffusion. In the present work, the kinetics of interfacial reactions are incorporated with the diffusion equation by relaxing the assumption of interfacial equilibria at the iron sulfide−oil interface {O}.

As explained previously, the mechanistic model for high-temperature sulfidation consists of distinguishable steps of transport or transformation (reaction) and rate equations for each of these steps. Typically, coefficients in these rate equations are phenomenological in nature, which must be determined by kinetic experiments. However, phenomenological coefficients determined for a particular crude oil are not useful to predict sulfidation rates for another crude oil. Therefore, the first milestone is to achieve an accurate simulation of trends in sulfidation rates.[28] In the next step, methods for determining accurate model coefficients should be developed.

It is well-known in refineries that oil phase sulfidation corrosion dramatically increases by the injection of H_2 for process purposes such as hydrotreating.[3,68] It can be hypothesized that the effect of H_2 can be evaluated once the mechanism of "H_2-free" sulfidation corrosion is known. In the literature of refinery sulfidation corrosion, experimental work on gaseous H_2S and H_2S + H_2 corrosion has often been referred to represent oil phase sulfidation.[3] However, the conditions of gaseous corrosion are quite different than liquid phase corrosion; hence, these experimental works are not cited herein.

The overall process of sulfidation corrosion can be classified mainly into two categories from the standpoint of kinetics:

https://doi.org/10.1021/acs.energyfuels.4c05072
Energy Fuels 2025, 39, 1844−1855

interfacial reactions generating or annihilating the charged point defects and their transport through the sulfide layer. The latter is commonly assumed to be rate-limiting, but experimentally observed linear mass loss versus time profile for oil phase sulfidation corrosion indicates interfacial reaction control.[30,49,69] It has been attempted to model interfacial reactions using Onsager's nonequilibrium thermodynamics by some researchers,[26,62] which is inappropriate for interfacial reactions especially when the standard Gibbs energy change of the reaction is significant.[49,63,69] Standard Gibbs energy change for the sulfur incorporation (reaction 2) involving organosulfur species can be significantly high due to obvious irreversibility implying that Gibbs energy dissipation shall also be high. Hence, this reaction must be modeled using theories of chemical kinetics. Reaction 3 can be assumed to be reversible with a relatively smaller standard Gibbs energy change and its rate may be modeled to be linearly proportional to the thermodynamic potential gradient.[63,69] However, the activation energy for reaction 3 is assumed to be low, which makes the reaction more rapid in comparison with other steps. Therefore, this reaction will be considered in equilibrium and not required to be modeled.

The standard Gibbs energy change for a transport process in an isotropic phase is always zero, although it is an activated process and the net transport in the direction of gradient occurs by application of thermodynamic potential difference.[49,70] Hence, a linear relation of rate with thermodynamic potential gradient is used to model the rates of transport processes according to Onsager's nonequilibrium thermodynamics.[49,62,70]

Initially, a significant charge accumulation occurs at the interfaces simultaneously with growing sulfide until the electrical potential is screened across the interfaces.[42,63] This is depicted by an inconspicuous nonlinear mass loss versus time trend in Figure 2. The charge accumulation at the interfaces results in the formation of a space charge. Theoretically, two space charge regions could form in the iron sulfide layer at each of the interfaces.[71,72] However, in the absence of experimental and literature data, the space charge at the iron sulfide− oil {O} interface has not been considered in this treatment. The initial period of charge accumulation is expected to be extremely short due to the high "chemical diffusivity" of pyrrhotite.[25] Therefore, the charge transport is only modeled for the steady state for long-term prediction of sulfidation corrosion rates. Therefore, a short nonlinear mass loss versus time trend[73,74] will not be captured by the model. Eventually, a linear to parabolic transition would occur as resistance to the transport increases with the growth of layer thickness.[75] In the case of oil phase sulfidation, the linear law is observed over an extended period because of the high chemical diffusivity of pyrrhotite. Thus, the kinetics of interfacial reactions need to be modeled using theories of chemical kinetics and subsequently specified as source/sink boundary conditions to the diffusion equation derived as per Wagner's theory.[59,64,69,76,77] It may be argued that the diffusion equation is not required in the model if the overall process is under interfacial reaction control. Since the interfacial reactions are sequentially connected with solid-state diffusion, any resistance to diffusion would directly affect the overall rate. Hence, interfacial kinetics needs to be added to the framework of solid-state diffusion.

Pressure and temperature are considered constant in the derivation of kinetics, which is typical for most systems in the field. Therefore, it can be derived from the fundamental property relation that the thermodynamic potential to drive the charge transport consists of chemical potential μ and electric potential $zF\phi$ for any charged defect. The sum of these potentials is defined as the electrochemical potential $\tilde{\mu} = \mu + zF\phi$ according to Guggenheim's formalism.[78]

The flux of individual charged defects V''_{Fe} and $h^{\bullet}$ can be specified using Onsager's postulate of linear nonequilibrium thermodynamics because the standard Gibbs energy change for the transport process is zero. According to Onsager's postulate, the flux is proportional to the sum of gradients of acting thermodynamic potentials.[62] Neglecting the "cross-effects" of potential gradients of the charges on each other, the flux of any charge can be written as follows.[62,63]

$$J_{V''} = -\beta_{V''}\frac{\partial \tilde{\mu}_{V''}}{\partial x} \text{ and } J_{h^{\bullet}} = -\beta_{h^{\bullet}}\frac{\partial \tilde{\mu}_{h^{\bullet}}}{\partial x}$$

Substituting the definition for the electrochemical potential explained before, the flux equations transform, as shown below.

$$J_{V''} = -\beta_{V''}\frac{\partial}{\partial x}(\mu_{V''} + z_{V''}F\phi) \text{and} J_{h^{\bullet}} = \beta_{h^{\bullet}}\frac{\partial}{\partial x}(\mu_{h^{\bullet}} + z_{h^{\bullet}}F\phi) \tag{5}$$

As the generation and annihilation of the vacancies and holes occur in a concerted manner after the charge accumulation phase, their transport is treated as a coupled chemical diffusion.[63] At a steady state, Wagner's coupled currents condition ($2J_{V''} = J_{h^{\bullet}}$) can be readily applied to eliminate the gradient of electric potential $\frac{\partial \phi}{\partial x}$ from the flux equation 5 to obtain a coupled chemical diffusion equation 6 for vacancies.[59]

$$J_{V''} = -\frac{\beta_{V''}\beta_{h^{\bullet}}}{\beta_{h^{\bullet}} + 4\beta_{V''}}\left(\frac{\partial \mu_{V''}}{\partial x} + 2\frac{\partial \mu_{h^{\bullet}}}{\partial x}\right) \tag{6}$$

Since pyrrhotite has metal-like conductivity,[25] it is reasonable to approximate the mobility of electron holes to be much greater than mobility of cation vacancies $\beta_{h^{\bullet}} \gg \beta_{V''}$,[25,46,67] which gives the following expression for the flux of vacancies.

$$J_{V''} = -\beta_{V''}\left(\frac{\partial \mu_{V''}}{\partial x} + 2\frac{\partial \mu_{h^{\bullet}}}{\partial x}\right) \tag{7}$$

The Gibbs−Duhem relation for constant pressure and temperature can be adopted to decrease the degrees of freedom of the system by one.[25] Since the Gibbs−Duhem relationship is derived from the fundamental property relation of thermodynamics and the extensivity related to thermodynamic potentials, it is considered applicable for an iron sulfide phase without interfacial equilibria. The Gibbs−Duhem relationship for the nonstoichiometric iron sulfide phase can be written as follows.

$$n_{V''}d\tilde{\mu}_{V''} + n_{h^{\bullet}}d\tilde{\mu}_{h^{\bullet}} + n_{Fe_{Fe}}d\mu_{Fe_{Fe}} + n_{S_S}d\mu_{S_S} = 0 \tag{8}$$

The value of the chemical potential of sulfur in an iron sulfide crystal μ_{S_S} at the steel surface is fixed by the solubility of sulfur in steel. Also in the present derivation, it has been already assumed that the sulfidation corrosion proceeds predominantly by the outward transport of iron whereas sulfur remains virtually immobile. Therefore, it can be inferred that its chemical potential μ_{S_S} does not change significantly throughout the thickness of the layer, i.e., $d\mu_{S_S} = 0$. Moreover,

https://doi.org/10.1021/acs.energyfuels.4c05072
Energy Fuels 2025, 39, 1844−1855

if δ is a fraction representing a deviation from the stoichiometry, $n_{V''} = \delta n_{S_S}$ and $n_{Fe_{Fe}} = (1-\delta)n_{S_S}$, assuming no sulfur vacancies in pyrrhotite. Neglecting space charge effects due to the higher conductivity of defects in pyrrhotite supports the assumption that a major portion of the sulfide layer is close to electroneutral, i.e., $n_{h^\bullet} \approx 2n_{V''}$. Substituting these conditions into equation 8

$$\delta n_{S_S} d\tilde{\mu}_{V''} + 2\delta n_{S_S} d\tilde{\mu}_{h^\bullet} + (1-\delta) n_{S_S} d\mu_{Fe_{Fe}} = 0$$

Using the definition of electrochemical potential for each component, $\tilde{\mu} = \mu + zF\phi$ in the above relation

$$\delta d(\mu_{V''} - 2F\phi) + 2\delta d(\mu_{h^\bullet} + F\phi) + (1-\delta) d\mu_{Fe_{Fe}} = 0$$

$$\delta d\mu_{V''} + 2\delta d\mu_{h^\bullet} + (1-\delta) d\mu_{Fe_{Fe}} = 0$$

$$d\mu_{Fe_{Fe}} = -\frac{\delta}{(1-\delta)}(d\mu_{V''} + 2d\mu_{h^\bullet}) \tag{9}$$

From equations 7 and 9:

$$J_{V''} = \frac{(1-\delta)\beta_{V''}}{\delta}\left(\frac{\partial \mu_{Fe_{Fe}}}{\partial x}\right) \tag{10}$$

It may be noted that the values of the chemical potential $\mu_{Fe_{Fe}}$ at the interfaces are dictated by the Gibbs energy dissipation by the respective interfacial chemical reaction. Equation 10 can be transformed into different useful forms as follows.

From the definition of the chemical potential, $\mu = \mu^{\ominus} + RT\ln a$ ($\mu^{\ominus}$= constant):

$$J_{V''} = \frac{(1-\delta)\beta_{V''}RT}{\delta}\left(\frac{\partial \ln a_{Fe_{Fe}}}{\partial x}\right) \tag{11}$$

It can be assumed for the sake of simplicity of the derivation that "cations" behave ideally so that activity can be simplified to concentration with respect to some standard value.[63]

$$J_{V''} = \frac{(1-\delta)\beta_{V''}RT}{\delta}\left(\frac{\partial \ln C_{Fe_{Fe}}}{\partial x}\right) \tag{12}$$

Mobility of vacancies can be substituted by diffusion coefficient using the Nernst−Einstein relation, $\beta_{V''} = C_{V''}D_{V''}/(RT)$.[63]

$$J_{V''} = \frac{(1-\delta)C_{V''}D_{V''}}{\delta}\left(\frac{\partial \ln C_{Fe_{Fe}}}{\partial x}\right) \tag{13}$$

Mobility of vacancies are equivalent to the mobilities of iron in the lattice.[63]

$$\beta_{V''} = \beta_{Fe_{Fe}} C_{V''}D_{V''} = C_{Fe_{Fe}}D_{Fe_{Fe}}$$

Using the above relation (equation 13)

$$J_{V''} = \frac{(1-\delta)C_{Fe_{Fe}}D_{Fe_{Fe}}}{\delta}\left(\frac{\partial \ln C_{Fe_{Fe}}}{\partial x}\right)$$

The flux of vacancies can be substituted by the flux of iron, i.e., $J_{V''} = -J_{Fe_{Fe}}$.

$$J_{Fe_{Fe}} = -\frac{(1-\delta)D_{Fe_{Fe}}}{\delta}\left(\frac{\partial C_{Fe_{Fe}}}{\partial x}\right)$$

The equation described above can be approximated in terms of differences.

$$J_{Fe_{Fe}} = -\frac{(1-\delta)D_{Fe_{Fe}}}{\delta}\left(\frac{\Delta C_{Fe_{Fe}}}{X}\right) \tag{14}$$

Here, $X = J_{Fe_{Fe}}\frac{MW_{FeS}}{\rho_{FeS}} \times 10^{-3} \times t$

Equation 14 resembles Fick's law of diffusion.[79] A relatively simpler and comprehensible end form of the transport equation has been reached to describe the basic kinetic trends of sulfidation corrosion. One may choose to use a more generic equation by relaxing the assumptions made during the derivation, if necessary.[26,64]

The concentrations of cations at respective interfaces are required to calculate the flux according to equation 14. The value of $C_{Fe_{Fe}}^{\{M\}}$ is fixed by an interfacial equilibrium previously assumed for the interface $\{M\}$. The sulfur incorporation reaction determines the value of $C_{Fe_{Fe}}^{\{O\}}$ at the iron sulfide−oil interface. This reaction may be analytically partitioned into several elementary steps to assign kinetic equations to each of them. However, this has not been attempted due to the lack of experimental evidence for the hypothesized mechanistic steps. Thus, the rate of sulfur incorporation $r^{\{O\}}$ at the iron sulfide-oil interface $\{O\}$ as per reaction 2 can be specified as follows which allows first-order dependence of rate with respect to the concentration of organosulfur compounds as illustrated earlier in Figure 3.[75]

$$r^{\{O\}} = -k^{\{O\}}C_{RSR}^{\{B\}}C_{Fe_{Fe}}^{\{O\}} \tag{15}$$

The rate constant $k^{\{O\}}$ in equation 15 may be modeled using traditional chemical kinetics. In steady state, the rates of charge transport and charge generation at the interface $\{O\}$ are equal as shown below and this relation will be used in obtaining the final mathematical expression for the corrosion rate.

$$J_{Fe_{Fe}} = r^{\{O\}} \tag{16}$$

Equations 14−16 form a complete system of equations for the kinetics of sulfidation corrosion.

Equations 14 and 15 are essentially the rate equations for the transport and reaction steps occurring in series. Therefore, it is possible to analyze their relationship with each other by analogy with a simple electrical circuit with two resistors $\mathcal{R}_J$ and $\mathcal{R}_r$ in a series representing transport and reaction steps, respectively. By analogy, resistances to transport and reaction steps can be defined as $\mathcal{R}_J \equiv \delta X/[(1-\delta)D_{Fe_{Fe}}]$ and $\mathcal{R}_r \equiv 1/k^{\{O\}}$ from equations 14 and 15, respectively. Qualitatively speaking, less reactive organosulfur compound means higher $\mathcal{R}_r$ and lower δ, meaning, lower $\mathcal{R}_J$ relative to $\mathcal{R}_r$. In that case, overall sulfidation kinetics would remain in the interfacial reaction control, leading to linear mass loss versus time trend, obtained by time integration of equation 15. This scenario corresponds to the present case of sulfidation corrosion by DDS which has a relatively lower reactivity than dimethyldisulfide (DMDS) used by the other researchers.[16,23] For highly reactive DMDS, the value of $\mathcal{R}_J$ would be higher relative to the value of $\mathcal{R}_r$ and the rate of the overall sulfidation process will be controlled diffusion of iron through the iron sulfide scale. In that case, the time-integration of (14) would lead to the parabolic mass loss/gain versus time trend as exhibited by the experimental data reported by the other researchers.[16,23]

https://doi.org/10.1021/acs.energyfuels.4c05072
Energy Fuels 2025, 39, 1844−1855

Chronological sequencing of rate-determining steps can be explained by referring to irreversible entropy generation by the transport process.[30] Increasing the thickness (X) of the corrosion product layer increases the resistance to chemical diffusion of charged defects according to the relation $\mathcal{R}_J = \delta X/[(1-\delta)D_{Fe_{Fe}}]$.[30] Since a thin layer does not provide much resistance to charge transport initially, the rate of interfacial reactions remains rate determining at the beginning, indicated by linear mass loss versus time trends.[28,30,75] Linear to parabolic transition occurs in the later stage when the thickness of iron sulfide is sufficiently high to provide more resistance to chemical diffusion.[75] This transition can often be significantly delayed due to the high chemical diffusivity of pyrrhotite and the lower reactivity of organosulfur compounds.

Simulation of mass loss versus time by the proposed model has been shown in Figure 8. Since the kinetic data in Figure 2

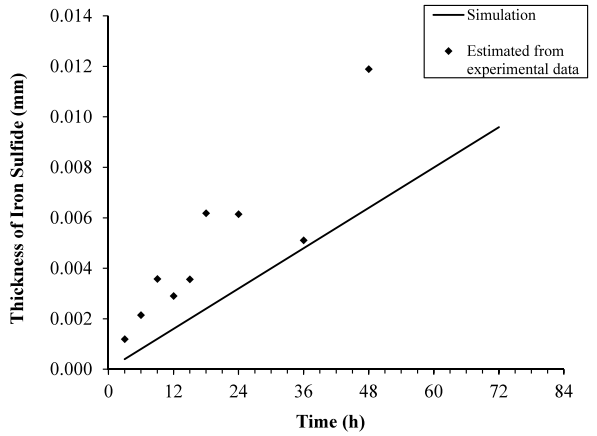

Figure 8. Simulated evolution of iron sulfide thickness compared with thicknesses estimated from experimental data in Figure 2 under the same experimental conditions. Model parameters: $k^{\{O\}} = 4.32 \times 10^{-10}$ m/s and $D_{Fe_{Fe}} = 3.11 \times 10^{-12}$ m^2/s.[80]

show interfacial reaction control, only the reaction rate constant $k^{\{O\}} = 4.32 \times 10^{-10}$ m/s has been obtained by fitting of data but no attempt is made to fit chemical diffusivity in the regression. The reference value for the diffusion coefficient used for the purpose of performing model simulations was calculated from the formulas derived by Herbert et al.[80] It should be noted that the diffusion coefficient for iron in iron sulfide depends on the gradient of the chemical potential of iron across the layer which ultimately depends on the activity of the organosulfur compound in the environment. Thus, the reference value of $D_{Fe_{Fe}} = 3.11 \times 10^{-12}$ m^2/s[80] used in the simulation may not represent the effective chemical diffusivity of iron sulfide formed during experiments. Therefore, a significant margin can be observed in Figure 8 between the experimentally estimated and simulated values of iron sulfide thicknesses. Simulation of iron sulfide thickness evolution before 3 h is avoided as it may fall in a "thin film regime" with completely different kinetics.

Initial linear kinetics also means that the "thickness" of the space charge is much lower compared to the thickness of the iron sulfide layer. Thus, the interfacial reaction kinetics is "independent" of the thermodynamic potential difference across the interface. The length of the linear period also depends on the molecular structure of the organosulfur species in the oil, which determines their reactivity, or alternatively the resistivity $\mathcal{R}_r \equiv 1/k^{\{O\}}$, and the free energy dissipation by the interfacial reaction.[75,81] If the free energy dissipation by the interfacial reaction of a given organosulfur molecule is negligible and the reactivity of the organosulfur compound is high, parabolic growth may be observed, as demonstrated using model simulations in Figure 9. Increasing reactivity of

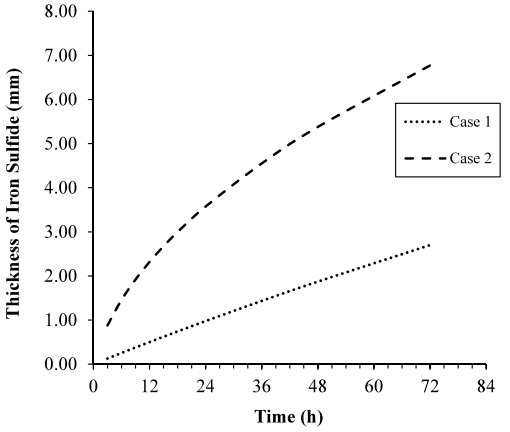

Figure 9. Simulated evolution of iron sulfide thickness using $D_{Fe_{Fe}} = 3.11 \times 10^{-12}$ m^2/s and model values of interfacial reaction rate constant $k^{\{O\}} = 1 \times 10^{-9}$ m/s for case 1, and 1×10^{-8} m/s for case 2 to illustrate the effect of reactivity of organosulfur compounds on kinetics. wt % S = 0.25 and T = 343 °C.

organosulfur compounds forces the kinetics to follow a parabolic trend as illustrated in Figure 9 by simulation using model values of the reaction rate constant higher than the one measured for DDS. In this case, the linear region could be too short to be noticeable. This explanation supports the parabolic trend identified by the other researchers referred to earlier.[15,23]

It is important to mention here that the convective diffusion of sulfide species in the oil phase has been assumed to be rapid because the rate of sulfidation has not been observed to be significantly affected by the velocity of an oil stream.[82] However, one can add a convective diffusion equation for organosulfur molecules to calculate their surface concentration.[83,84]

CONCLUSIONS

Linear mass loss versus time trend exhibited in high-temperature sulfidation experiments in the oil phase inferred that the underlying overall kinetics was in interfacial control. Therefore, mechanisms of interfacial reactions were proposed, and the associated kinetic equations were derived. Interfacial reaction rate equations were incorporated with the solid-state diffusion equation for comprehensive kinetic modeling of sulfidation corrosion. Experimentally observed linear mass loss versus time trend for sulfidation corrosion of carbon steel by dodecylsulfide (DDS) can be explained by derived kinetics equations. It could also explain that the sulfidation by more reactive organosulfur compounds would follow a parabolic law. The model can also capture the characteristic phenomena of a linear to parabolic transition with increasing thickness of the iron sulfide layer as illustrated by the model simulations. A straightforward computational code for the simplified form of the model can be utilized for the prediction of the sulfidation corrosion rate in the oil refining industry. Values of

https://doi.org/10.1021/acs.energyfuels.4c05072
Energy Fuels 2025, 39, 1844−1855

phenomenological coefficients for the model can be obtained by kinetic measurements, as described in this article.

AUTHOR INFORMATION

Corresponding Author

David Young − *Institute for Corrosion and Multiphase Technology, Department of Chemical & Biomolecular Engineering, Ohio University, Athens, Ohio 45701, United States*; orcid.org/0000-0002-1077-9586; Phone: +1-740-593-9944; Email: youngd1@ohio.edu

Authors

Ishan P. Patel − *Institute for Corrosion and Multiphase Technology, Department of Chemical & Biomolecular Engineering, Ohio University, Athens, Ohio 45701, United States*

Gheorghe Bota − *Institute for Corrosion and Multiphase Technology, Department of Chemical & Biomolecular Engineering, Ohio University, Athens, Ohio 45701, United States*

Complete contact information is available at: https://pubs.acs.org/10.1021/acs.energyfuels.4c05072

Author Contributions

The manuscript was written through contributions of all authors. All authors have given approval to the final version of the manuscript.

Notes

The authors declare no competing financial interest.

Kröger−Vink Notations (representing lattice species in the reactions): in $\mathbf{A}_S^C$, A is a structural element (Fe, S, V = vacancy, h = electron hole in valence band, e = electron in conduction band); *C* is a relative charge (• = positive and ′ = negative); subscript S is a lattice site (Fe, S, or i = interstitial).

ACKNOWLEDGMENTS

This work was supported by Naphthenic Acid Corrosion Joint Industry Project (NAP JIP) in the Institute for Corrosion and Multiphase Technology, Ohio University.

PHYSICAL AND PHENOMENOLOGICAL QUANTITIES

k_p= parabolic rate constant
k_l= linear rate constant
$\tilde{\mu}$= electrochemical potential of any charge
μ= chemical potential of any charge
ϕ= electric potential at any location
F= Faraday's constant
J= flux of particles in mol/area/time
x= distance perpendicular to the surface of steel
β= mobility of charge in the ionic crystal
z= charge number
a= thermodynamic activity
D= diffusion coefficient
R= universal gas constant
T= absolute temperature
n= quantity of any lattice component
δ= fraction of cation defects indicating nonstoichiometry
C= concentration
k= rate constant for interfacial reaction
X= thickness of the iron sulfide layer
r= rate of heterogeneous reaction
$MW_{Fe_{1-\delta}S}$= molecular weight of pyrrhotite
$\rho_{Fe_{1-\delta}S}$= density of pyrrhotite
t= time
$\mathcal{R}_j$= resistance provided by diffusion process
$\mathcal{R}_r$= resistance provided by reaction

SUBSCRIPTS

V'' negatively charged cation vacancy
$h^\bullet$ positively charged electron hole in the valence band
Fe_{Fe} iron in the lattice at cation location
S_S sulfur in the lattice at anion location

SUPERSCRIPTS

$\ominus$ standard state

CURLY BRACKETS REPRESENT THE LOCATIONS

$\{B\}$ in the bulk oil phase
$\{O\}$ at the iron sulfide−oil interface
$\{M\}$ at the iron−iron sulfide interface

REFERENCES

(1) Foroulis, Z. A. High Temperature Degradation of Structural Materials in Environments Encountered in the Petroleum and Petrochemical Industries: Some Mechanistic Observations. *Anti-Corros. Methods Mater.* **1985**, *32* (11), 4−9.

(2) American Petroleum Institute. *Damage Mechanisms Affecting Fixed Equipment in the Refining Industry*; API RP 2020 *571*.

(3) American Petroleum Institute. *Guidelines for Avoiding Sulfidation (Sulfidic) Corrosion Failures in Oil Refineries*; API, 2019 *939-C*.

(4) Bravo-Méndez, J.; González-Velázquez, J. L.; Domínguez-Aguilar, M. A.; Rivas- López, D. I. High-Temperature Corrosion of a UNS K03006 Steel Pipe in a Crude Oil Vacuum Residue Distillation Unit. *Eng. Fail. Anal.* **2018**, *92*, 149−162.

(5) U.S. Chemical Safety Board *Chevron Richmond Refinery Pipe Rupture and Fire*; 2012−03-I-CA, U.S. Chemical Safety Board: Richmond, CA, 2015. https://www.csb.gov/chevron-richmond-refinery-fire/ (accessed 2024−07−27).

(6) Exponent Failure Analysis Associates *Silver Eagle Refinery Explosion Investigation: Metallurgical Analysis*; Houston, TX: U. S. Chemical Safety Board, 2013. https://www.csb.gov/silver-eagle-refinery-flash-fire-and-explosion-and-catastrophic-pipe-explosion/ (accessed 2024−07−27).

(7) Sorell, G.; Hoyt, W. B. Collection and Correlation of High Temperature Hydrogen Sulfide Corrosion Data—A Contribution to the Work of NACE Task Group T-5B-2 on Sulfide Corrosion at High Temperatures and Pressures in the Petroleum Industry from: The M. W. Kellogg Co., New York, N. Y. *Corrosion* **1956**, *12* (5), 33−54.

(8) NACE International. *Overview of Sulfidation (Sulfidic) Corrosion in Petroleum Refining Hydroprocessing Units (34103)*; NACE Task Group 176; 2014. https://store.ampp.org/nace-publication-34103-2014- (accessed 2024−07−27).

(9) Yoon, Y.; Srinivasan, S. A Review of Naphthenic Acid Corrosion and Sulfidic Corrosion in Crude Oil Refining Applications. In *CORROSION 2019*, Nashville, Tennessee, March 24−28, 2019; NACE International, Publications Division: Houston, TX, 2019; NACE-2019−13443.

(10) Toba, K.; Miyamoto, S.; Tokuoka, S. A New Prediction Tool for Sulfidation Corrosion in Crude Units. In *CORROSION 2021 Virtual Conference & Expo*; The Association for Materials Protection and Performance, April 2021; NACE-2021−16762.

(11) Wing, A.; Robbins, W.; Buchheim, G.; Sapienza, F. Introducing an Innovative Simultaneous Naphthenic Acid, Sulfidation and Mass Transport Corrosion Model for Crudes and Sidestreams. In *CORROSION Virtual Conference & Expo 2021*, April 19−30, 2021; 16755.

(12) Hau, J. Predicting Sulfidic and Naphthenic Acid Corrosion. *Corrosion* **2009**, *65* (12), 831−844.
(13) Jin, P.; Robbins, W.; Bota, G. High-Temperature Corrosion by Carboxylic Acids and Sulfidation under Refinery Conditions—Mechanism, Model, and Simulation. *Ind. Eng. Chem. Res.* **2018**, *57* (12), 4329−4339.
(14) Al-Moubaraki, A. H.; Obot, I. B. Corrosion Challenges in Petroleum Refinery Operations: Sources, Mechanisms, Mitigation, and Future Outlook. *J. Saudi Chem. Soc.* **2021**, *25* (12), No. 101370.
(15) El Kamel, M.; Galtayries, A.; Vermaut, P.; Albinet, B.; Foulonneau, G.; Roumeau, X.; Roncin, B.; Marcus, P. Sulfidation Kinetics of Industrial Steels in a Refinery Crude Oil at 300 °C: Reactivity at the Nanometer Scale. *Surf. Interface Anal.* **2010**, *42* (6−7), 605−609.
(16) Sharifi-Asl, S.; Liang, A.; Cooke, D.; Chapman, D. R.; Chaloner-Gill, B.; Kuperman, A. E. High-Temperature Sulfidic Corrosion of Carbon Steel in Model Oil/Sulfur Compound Blends. In *CORROSION 2017*, March 26−30, 2017; NACE International, Publications Division: Houston, TX, 2017; NACE-2017−8909.
(17) Ho, T. Y.; Rogers, M. A.; Drushel, H. V.; Koons, C. B. Evolution of Sulfur Compounds in Crude Oils. *Am. Assoc. Pet. Geol. Bull.* **1974**, *58* (11), 2338−2348.
(18) Lobodin, V. V.; Robbins, W. K.; Lu, J.; Rodgers, R. P. Separation and Characterization of Reactive and Non-Reactive Sulfur in Petroleum and Its Fractions. *Energy Fuels* **2015**, *29* (10), 6177−6186.
(19) Rodgers, R. P.; Robbins, W. K.; Lobodin, V. V. Determination of the Distribution of Reactive and Non-Reactive Sulfur in Petroleum and Its Fractions, US 20160025699 A1, 2018.
(20) Lyapina, N. K.; Marchenko, G. N.; Parfenova, M. A.; Galkin, E. G.; Nugumanov, R. M.; Grishina, R. E. Organic Sulfur Compounds in Petroleum of the Arkhangel'sko-Tanaiskoe Field. *Pet. Chem.* **2010**, *50* (1), 31−41.
(21) Piehl, R. L. Correlation of Corrosion in a Crude Distillation Unit with Chemistry of the Crudes. *Corrosion* **1960**, *16* (6), 305t−307t.
(22) Foroulis, Z. A. Kinetics and Mechanism of the Reaction of Iron with Sulfur Vapor in the Temperature Range of 250 to 500°C. *Mater. Corros.* **1978**, *29* (6), 385−393.
(23) Qu, D. R.; Zheng, Y. G.; Jing, H. M.; Yao, Z. M.; Ke, W. High Temperature Naphthenic Acid Corrosion and Sulphidic Corrosion of Q235 and 5Cr1/2Mo Steels in Synthetic Refining Media. *Corros. Sci.* **2006**, *48* (8), 1960−1985.
(24) Kröger, F. A.; Vink, H. J. Relations between the Concentrations of Imperfections in Crystalline Solids. In *Solid State Phys.*; Seitz, F., Turnbull, D., Eds.; Academic Press, 1956; Vol. *3*, pp 307−435.
(25) Young, D. J. *High Temperature Oxidation and Corrosion of Metals*, 2nd ed.; Elsevier, 2016.
(26) Ramanathan, R.; Voorhees, P. W. Departures from Local Interfacial Equilibrium during Metal Oxidation. *Phys. Rev. Mater.* **2020**, *4* (11), No. 113401.
(27) Per, Kofstad. *High Temperature Oxidation of Metals*, 1st ed.; John Wiley and Sons, 1966.
(28) Patel, I.; Bota, G.; Young, D. Mechanistic Insights into Refinery Sulfidation Corrosion. In *AMPP Annual Conference + Expo 2023, Proceedings of Refining Industry Corrosion Symposium*, Denver, CO, March 19−23, 2023; C2023−19107.
(29) Tammann, G. Über Anlauffarben von Metallen. *Z. Anorg. Allg. Chem.* **1920**, *111* (1), 78−89.
(30) Schmalzried, H. Chemical Kinetics at Solid-Solid Interfaces. *Pure Appl. Chem.* **2000**, *72* (11), 2137−2147.
(31) Hsu, C. S.; Dechert, G. J.; Robbins, W. K.; Fukuda, E. K. Naphthenic Acids in Crude Oils Characterized by Mass Spectrometry. *Energy Fuels* **2000**, *14* (1), 217−223.
(32) Babaian-Kibala, E.; Nugent, M. J. Naphthenic Acid Corrosion Literature Survey. In *CORROSION 99*, San Antonio, Texas, April 25−30, 1999; NACE International, Publications Division: Houston, TX, 1999; NACE-99378.
(33) Slavcheva, E.; Shone, B.; Turnbull, A. Review of Naphthenic Acid Corrosion in Oil Refining. *Br. Corros. J.* **1999**, *34* (2), 125−131.
(34) Yépez, O. Influence of Different Sulfur Compounds on Corrosion Due to Naphthenic Acid. *Fuel* **2005**, *84* (1), 97−104.
(35) Patel, I.; Bota, G.; Young, D. Physicochemical Description of Refinery High Temperature Naphthenic Acid Corrosion. In *AMPP Annual Conference + Expo 2024, Proceedings of Oil Refining Industry Corrosion Symposium*, New Orleans, LA, March 3−7, 2024; C2024−20988.
(36) Jin, P.; Nesic, S. Mechanism of Magnetite Formation in High Temperature Naphthenic Acid Corrosion by Crude Oil Fractions. *Corros. Sci.* **2017**, *115*, 93−105.
(37) Bota, G.; Kurapati, Y.; Jin, P.; Robbins, W. Sulfur/TAN Ratio Effect on Iron Sulfide (FeS) Scale Properties Challenged in Continuous Oil Flow. In *CORROSION 2019, Proceedings of Refining Industry Corrosion Symposium*, Nashville, Tennessee, USA, March 24−28, 2019; NACE International, Publications Division: Houston, TX, *2019*, C2019−13490.
(38) Bota, G. M.; Qu, D.; Nesic, S.; Wolf, H. A. Naphthenic Acid Corrosion of Mild Steel in the Presence of Sulfide Scales Formed in Crude Oil Fractions at High Temperature. In *CORROSION 2010*, San Antonio, Texas, March 14−18, 2010; NACE International, Publications Division: Houston, TX, 2010; 10353.
(39) Jin, P.; Wolf, H. A.; Srdjan, N. Analysis of Corrosion Scales Formed on Steel at High Temperatures in Hydrocarbons Containing Model Naphthenic Acids and Sulfur Compounds. In *CORROSION 2014*, San Antonio, Texas, USA, March 9−13, 2014; NACE International, Publications Division: Houston, TX, NACE-2014−4075.
(40) Jin, P.; Nesic, S.; Wolf, H. A. Analysis of Corrosion Scales Formed on Steel at High Temperatures in Hydrocarbons Containing Model Naphthenic Acids and Sulfur Compounds. *Surf. Interface Anal.* **2015**, *47* (4), 454−465.
(41) Patel, I.; Bota, G.; Jin, P.; Young, D. Mechanism and Rate Law for High-Temperature Carboxylic Acid Corrosion of Steels. *Energy Fuels* **2024**, *38* (12), 10744−10754.
(42) Maier, J. Defect Chemistry and Ionic Conductivity in Thin Films. *Solid State Ion.* **1987**, *23* (1−2), 59−67.
(43) Fogler, H. S. *Essentials of Chemical Reaction Engineering*; Prentice Hall: Upper Saddle River, NJ, 2011.
(44) Swalin, R. A. *Thermodynamics of Solids*, 1st ed.; John Wiley and Sons, 1962.
(45) Gates-Rector, S.; Blanton, T. The Powder Diffraction File: A Quality Materials Characterization Database. *Powder. Diffr.* **2019**, *34* (4), 352−360.
(46) Vaughan, D. J.; Craig, J. R. *Mineral Chemistry of Metal Sulfides*; Cambridge University Press: Cambridge [Eng.]: New York, 1978.
(47) Maier, J. Defect Chemistry: Composition, Transport, and Reactions in the Solid State; Part I: Thermodynamics. *Angew. Chem., Int. Ed. Engl.* **1993**, *32* (3), 313−335.
(48) Anand, S.; Toriyama, M. Y.; Wolverton, C.; Haile, S. M.; Snyder, G. J. A Convergent Understanding of Charged Defects. *Acc. Mater. Res.* **2022**, *3* (7), 685−696.
(49) Maier, J. *Physical Chemistry of Ionic Materials: Ions and Electrons in Solids; Wiley: Chichester*; Hoboken: NJ, 2004.
(50) Jost, W. Diffusion and Electrolytic Conduction in Crystals (Ionic Semiconductors). *J. Chem. Phys.* **1933**, *1* (7), 466−475.
(51) Mott, N. F.; Littleton, M. J. Conduction in Polar Crystals. I. Electrolytic Conduction in Solid Salts. *Trans. Faraday Soc.* **1938**, *34*, 485.
(52) Oleksak, R. P.; Kapoor, M.; Perea, D. E.; Holcomb, G. R.; Doğan, Ö. N. The Role of Metal Vacancies during High-Temperature Oxidation of Alloys. *Npj Mater. Degrad.* **2018**, *2* (1), 25.
(53) Lübbehusen, M.; Mehrer, H. Self-Diffusion in α-Iron: The Influence of Dislocations and the Effect of the Magnetic Phase Transition. *Acta Metall. Mater.* **1990**, *38* (2), 283−292.
(54) Zhang, B.Calculation of Self-Diffusion Coefficients in Iron. *AIP Adv.* 2014, *4*, 1, .

https://doi.org/10.1021/acs.energyfuels.4c05072
Energy Fuels 2025, 39, 1844−1855

(55) Maurice, V.; Despert, G.; Zanna, S.; Bacos, M.-P.; Marcus, P. Self-Assembling of Atomic Vacancies at an Oxide/Intermetallic Alloy Interface. *Nat. Mater.* **2004**, *3* (10), 687−691.
(56) Kolb, D. Reconstruction Phenomena at Metal-Electrolyte Interfaces. *Prog. Surf. Sci.* **1996**, *51* (2), 109−173.
(57) Schmickler, W. Electronic Effects in the Electric Double Layer. *Chem. Rev.* **1996**, *96* (8), 3177−3200.
(58) Luo, L.; Li, L.; Schreiber, D. K.; He, Y.; Baer, D. R.; Bruemmer, S. M.; Wang, C. Deciphering Atomistic Mechanisms of the Gas-Solid Interfacial Reaction during Alloy Oxidation. *Sci. Adv.* **2020**, *6* (17). DOI: .
(59) Wagner, C. Beitrag Zur Theorie Des Anlaufvorgangs. *Z. Phys. Chem.* **1933**, *21B* (1), 25.
(60) Wagner, C. Theoretical Analysis of the Diffusion Processes Determining the Oxidation Rate of Alloys. *J. Electrochem. Soc.* **1952**, *99* (10), 369.
(61) Wagner, C. Equations for Transport in Solid Oxides and Sulfides of Transition Metals. *Prog. Solid State Chem.* **1975**, *10*, 3−16.
(62) Onsager, L. Reciprocal Relations in Irreversible Processes. *I. Phys. Rev.* **1931**, *37* (4), 405−426.
(63) Maier, J. Defect Chemistry: Composition, Transport, and Reactions in the Solid State; Part II: Kinetics. *Angew. Chem., Int. Ed. Engl.* **1993**, *32* (4), 528−542.
(64) Cheng, T.-L.; Wen, Y.-H.; Hawk, J. A. Diffuse-Interface Modeling and Multiscale-Relay Simulation of Metal Oxidation Kinetics—With Revisit on Wagner's Theory. *J. Phys. Chem. C* **2014**, *118* (2), 1269−1284.
(65) Xu, Z.; Rosso, K. M.; Bruemmer, S. Metal Oxidation Kinetics and the Transition from Thin to Thick Films. *Phys. Chem. Chem. Phys.* **2012**, *14* (42), 14534.
(66) Worm, H.-U.; Clark, D.; Dekkers, M. J. Magnetic Susceptibility of Pyrrhotite: Grain Size, Field and Frequency Dependence. *Geophys. J. Int.* **1993**, *114* (1), 127−137.
(67) Pearce, C. I. Electrical and Magnetic Properties of Sulfides. *Rev. Mineral Geochem.* **2006**, *61* (1), 127−180.
(68) Samans, C. H. Review of High-Temperature Sulfidic Corrosion in Petroleum Refining. In *Fall Meeting of Electrochemical Society*; Foroulis, Z. A., Ed.; The Electrochemical Society: Detroit, MI, USA, 1969; pp 211−223.
(69) Kim, K.; Sherman, Q. C.; Aagesen, L. K.; Voorhees, P. W. Phase-Field Model of Oxidation: Kinetics. *Phys. Rev. E* **2020**, *101* (2), No. 022802.
(70) Rickert, H. Mobility, Diffusion and Partial Conductivity of Ions and Electrons. In *Electrochemistry of Solids*; Springer-Verlag, 1982; pp 79−117. .
(71) Otero, R.; Vázquez de Parga, A. L.; Gallego, J. M. Electronic, Structural and Chemical Effects of Charge-Transfer at Organic/Inorganic Interfaces. *Surf. Sci. Rep.* **2017**, *72* (3), 105−145.
(72) Cheng, T.-L.; Wen, Y.-H. Toward a Quantitative Understanding of the Electric Field in Thermal Metal Oxidation and a Self-Consistent Wagner Theory. *J. Phys. Chem. Lett.* **2014**, *5* (13), 2289−2294.
(73) Ramanarayanan, T. A.; Smith, S. N. Corrosion of Iron in Gaseous Environments and in Gas-Saturated Aqueous Environments. *Corrosion* **1990**, *46* (1), 66−74.
(74) Haycock, E. W. Transitions from Parabolic to Linear Kinetics in Scaling of Metals. *J. Electrochem. Soc.* **1959**, *106* (9), 771.
(75) Pettit, F. S.; Wagner, J. B. Transition from the Linear to the Parabolic Rate Law during the Oxidation of Iron to Wüstite in CO-CO2Mixtures. *Acta Metall.* **1964**, *12* (1), 35−40.
(76) Sherman, Q. C.; Voorhees, P. W. Phase-Field Model of Oxidation: Equilibrium. *Phys. Rev. E* **2017**, *95* (3), No. 032801.
(77) Fromhold, A. T. Kinetics of Oxide Film Growth on Metal Crystals—I. *J. Phys. Chem. Solids* **1963**, *24* (9), 1081−1092.
(78) Guggenheim, E. A. The Conceptions of Electrical Potential Difference between Two Phases and the Individual Activities of Ions. *J. Phys. Chem.* **1929**, *33* (6), 842−849.
(79) Shewmon, P. G. *Diffusion in Solids*, Second ed.; Springer International Publishing: Imprint: Springer: Cham, 2016.
(80) William Herbert, F.; Krishnamoorthy, A.; Rands, L.; Van Vliet, K. J.; Yildiz, B. Magnetic Diffusion Anomaly at the Néel Temperature of Pyrrhotite, $Fe_{1-x}S$. *Phys. Chem. Chem. Phys.* **2015**, *17* (16), 11036−11041.
(81) Bredesen, R.; Kofstad, P. On the Oxidation of Iron in CO_2 + CO Mixtures. III: Coupled Linear Parabolic Kinetics. *Oxid. Met.* **1991**, *36* (1−2), 25−56.
(82) American Petroleum Institute *Risk-Based Inspection Technology, Downstream Segment*; API *581*, 2020.
(83) Patel, I.; Bota, G.; Young, D. Evaluation of Reactive Sulfur for Improved Corrosion Predictions in Oil Refineries. In *AMPP Annual Conference + Expo 2022, Proceedings of Oil Refining Industry Corrosion Symposium*, San Antonio, TX, March 6−10, 2022; C2022−18039.
(84) Bota, G. M. Corrosion of Steel at High Temperature in Naphthenic Acid and Sulfur Containing Crude Oil Fractions. Ph.D. Dissertation, Ohio University: Athens, OH, 2010. http://rave.ohiolink.edu/etdc/view?acc_num=ohiou1289941947 (accessed 2019−10−25).